Relativistic polytropic spheres with electric charge: Compact stars, compactness and mass bounds, and quasiblack hole configurations

José D. V. Arbañil[1,*] and Vilson T. Zanchin[2,†]

[1]Departamento de Ciencias, Universidad Privada del Norte, Avenida Alfredo Mendiola 6062, Urbanización Los Olivos, Lima, Peru

[2]Centro de Ciências Naturais e Humanas, Universidade Federal do ABC, Avenida dos Estados 5001, 09210-580 Santo André, São Paulo, Brazil

(Received 17 October 2017; published 25 May 2018)

We study the static equilibrium configurations of uncharged and charged spheres composed by a relativistic polytropic fluid, and we compare with those of spheres composed by a nonrelativistic polytropic fluid, the later case being already studied in a previous work [J. D. Arbañil, P. S. Lemos, and V. T. Zanchin, Phys. Rev. D **88**, 084023 (2013)]. An equation of state connecting the pressure p and the energy density ρ is assumed. In the nonrelativistic fluid case, the connection is through a nonrelativistic polytropic equation of state, $p = \omega\rho^{\gamma}$, with ω and γ being respectively the polytropic constant and the polytropic exponent. In the relativistic fluid case, the connection is through a relativistic polytropic equation of state, $p = \omega\delta^{\gamma}$, with $\delta = \rho - p/(\gamma - 1)$, and δ being the rest-mass density of the fluid. For the electric charge distribution, we assume that the charge density ρ_e is proportional to the energy density ρ, $\rho_e = \alpha\rho$, with α being a constant such that $0 \leq |\alpha| \leq 1$. The study is developed by integrating numerically the hydrostatic equilibrium equation. Some properties of the charged spheres such as the gravitational mass, the total electric charge, the radius, the surface redshift, and the speed of sound are analyzed by varying the central rest-mass density, the charge fraction, and the polytropic exponent. In addition, some limits that arise in general relativity, such as the Chandrasekhar limit, the Oppenheimer-Volkoff limit, the Buchdahl bound, and the Buchdahl-Andréasson bound are studied. It is confirmed that charged relativistic polytropic spheres with $\gamma \to \infty$ and $\alpha \to 1$ saturate the Buchdahl-Andréasson bound, thus indicating that it reaches the quasiblack hole configuration. We show by means of numerical analysis that, as expected, the major differences between the two cases appear in the high energy density region.

DOI: 10.1103/PhysRevD.97.104045

I. INTRODUCTION

A. Uncharged spheres: Equations of state and mass bounds

In the study of stars, both in Newtonian gravitation and in general relativity, it is usual to model the matter by a perfect fluid. Such a fluid is fully characterized by its energy density ρ and pressure p, besides the speed of sound in it. In general, to close the system of equations, an equation of state relating the pressure to the energy density of the fluid is specified. Since Eddington [1], a polytropic equation of state has been assumed to build analytically simple star models. Such an equation relates the pressure and energy density by a power law of the form

$$p = \omega\rho^{\gamma}, \tag{1}$$

where ω and γ are respectively the polytropic constant and the polytropic exponent. Such a relation, which we call EoS 1, is derived in Newtonian fluid mechanics, in which case ρ is the mass density, but it is a good approximation for relativistic fluids as long as the energy density is sufficiently small (see, e.g., [2]).

The equation of state (1) has been employed in several contexts. A fact of interest here is that the first bound for the mass of a compact object was established, when studying white dwarfs, by using such a polytropic equation of state [3,4]. As a matter of fact, Chandrasekhar used EoS 1 (1) with $\gamma = 4/3$. Applying the laws of Newtonian gravitation, he found that the radius of the configuration decreases with growing of the energy density, and it shrinks to zero for a mass of approximately 1.44 $M_{\odot}$. This is the Chandrasekhar limit.

As in Newtonian gravitation, in the context of general relativity there are also mass bounds for compact objects. Studies in this direction were performed by Tolman [5] and Oppenheimer and Volkoff [6]. In their works, they showed that a mass limit can be also achieved in neutron stars. This mass limit, known as Oppenheimer-Volkoff limit, appears when the neutron star pressure is sufficiently large. In their

*Email: jose.arbanil@upn.pe
†Email: zanchin@ufabc.edu.br

works, Tolman [5] and Oppenheimer and Volkoff [6] wrote the gradient pressure in a very convenient form. This equation is known as the hydrostatic equilibrium equation or Tolman-Oppenheimer-Volkoff (TOV) equation.

EoS 1 and the TOV equation were used together for the first time by Tooper [7]. He discussed the structure of polytropic stars (polytropes) through the numerical integration of the TOV equation. Although the equation of state (1) describes spherical objects in a very simple manner, its use has some drawbacks. At very high pressures, it leads to obtaining values of the sound speed higher than the speed of light, violating the principle of causality. Thus, it is understood that a generalization of EoS 1 is required. The most reasonable generalization of the polytropic equation of state was given by Tooper in [8]. He showed that the pressure and the energy density of the generalized polytropic equation of state obey the relations

$$p = \omega\delta^{\gamma},$$
$$\rho = \delta + p/(\gamma - 1), \tag{2}$$

respectively, where δ represents the rest-mass density. In the preset work, Eq. (2) is referred to as EoS 2. Equations of state of the form (2) have been used to study neutron stars, in which the neutrons are nonrelativistic, and white dwarfs, in which the electron gas is extremely relativistic (see, e.g., [8]). For white dwarf models, where the fluid pressure is small in comparison to the energy density, EoS 2 is equivalent to EoS 1, because in that situation we may neglect the pressure in the second term on the right-hand side of Eq. (2) and take $\delta \simeq \rho$. The equilibrium configurations determined with EoS 2 are named after Thorne [2] as the relativistic polytropic models or relativistic polytropes (for short); henceforth, these names will be used throughout this work. It is important to mention that a brief comparison between nonrelativistic polytropes and relativistic polytropes without and with cosmological constant have been considered respectively in [9] (see also [10,11]) and [12], and for nonisotropic fluids in [13].

B. Charged spheres and the TOV method

The first analysis on charged objects by means of the TOV method were developed by Bekenstein in [14]. From then on, many different works addressing the influence of electric charge and electric fields in the structure of compact objects were reported. Among them, we find studies on the equilibrium configurations of charged compact stars where the fluid follows EoS 1, e.g., [15–18]. In Refs. [16,17] the authors focused on studying the effects of the electric charge on the structure of compact cold stars. In these works, the modified TOV equation was solved considering EoS 1 with $\gamma = 5/3$ and a charge density proportional to the energy density, $\rho_e = \alpha\rho$ (α being a constant that obeys the constraint $0 \leq \alpha \leq 1$). Arbañil, Lemos and Zanchin (ALZ) in [18] also studied the structure of electrically charged objects considering EoS 1, varying the polytropic exponent γ, and with the charge distribution given by $\rho_e = \alpha\rho$. The mass bounds for these charged compact objects were also investigated in the same work. The authors found that extremely charged polytropic stars with $\gamma \to \infty$ are structures with the total charge Q close to the total mass M, $Q \simeq M$, and with radius R close to the gravitational radius R_+, $R \simeq R_+ \simeq M$. This indicates that the solutions are close to the quasiblack hole configurations (see, e.g., [19]).

C. Compactness bounds and quasiblack hole configurations

Uncharged compact objects in general relativity obey the Buchdahl bound [20]. This bound states that the radius R and the gravitational mass M of a sphere of perfect fluid in hydrostatic equilibrium satisfying reasonable physical conditions satisfies the inequality $R/M \geq 9/4$. If a star shrinks to a size that violates this bound, it eventually turns into a black hole. This bound is saturated by the interior Schwarzschild solution in the limit of infinite central pressure [21] (see also [22]). That is to say, the Buchdahl bound saturated by an incompressible fluid with an infinite central pressure gives the upper limit of the bound, $R/M = 9/4$. The Buchdahl bound is a general result in the sense that it is independent of the equation of state used.

The charged compact objects in general relativity coupled to Maxwell electromagnetism satisfy the Buchdahl-Andréasson bound [23]. This bound states that a hydrostatic equilibrium configuration of charged fluid matter obeys the relation

$$\frac{R}{M} \geq \frac{9}{\left(1 + \sqrt{1 + 3Q^2/R^2}\right)^2}. \tag{3}$$

As shown in Ref. [24], the Buchdahl-Andréasson bound is saturated by the Guilfoyle solutions [25] for charged spheres in the limit where the central pressure attains arbitrarily large values, in full analogy to the Schwarzschild interior limit. As verified in Refs. [18,22], charged fluids satisfying the nonrelativistic polytropic equation of state and a charged incompressible fluid do not saturate the Buchdahl-Andréasson bound. In the limit of extremely charged objects, this bound corresponds to the quasiblack hole configuration.

It is important to stress that the quasiblack hole limit is found using different equations of state and different electric charge distributions. Such limiting solutions have been found, e.g., for an incompressible fluid with a distribution of electric charge which follows a particular function of the radial coordinate [26–28], and when the charge density is proportional to the energy density [18,22]. Quasiblack holes have also been obtained in works that use an equation of state for electrically charged dust ($p = 0$) [29,30], and also in works that use the Cooperstock–de la Cruz–Florides [25,31,32] equation of state, as in

Refs. [24,33,34]. The general properties of quasiblack holes were defined in [19,35].

D. This work

We are interested in analyzing the equilibrium configurations of fluid spheres in the presence or absence of electric charge, taking into account the relativistic polytropic equation of state (2). The results found here are compared with the ones found using the nonrelativistic polytropic equation of state (1) [18]. For short, we refer to the respective configurations as nonrelativistic polytropic stars (or nonrelativistic polytropes) and relativistic polytropic stars (or relativistic polytropes). Very compressed objects, the compactness bounds and quasiblack hole limits are the main objects of interest here.

The article is structured according as follows. In Sec. II we write the TOV equation with the inclusion of the electric charge. The equation of state, the charge density profile and the boundary conditions are also considered in such a section. Section III is dedicated to comparing the structure of charged relativistic polytropes with the charged nonrelativistic polytropes for different values of polytropic exponent γ. We analyze the Chandrasekhar limit, the Oppenheimer-Volkoff limit, the Buchdahl bound and the Buchdahl-Andréasson bound. Some physical properties of the fluid for an arbitrarily large polytropic exponent γ are given in Sec. IV. The dependence of the speed of sound as a function of the polytropic exponent is accomplished in Sec. V. In Sec. VI we study the quasiblack hole limit and the redshift on the surface of a quasiblack hole. In Sec. VII we conclude.

II. GENERAL RELATIVISTIC CHARGED PERFECT FLUID

A. Equations of structure

The line element for a static spherically symmetric spacetime, in Schwarzschild coordinates, is

$$ds^2 = -Bdt^2 + Adr^2 + r^2 d\theta^2 + r^2 \sin^2\theta d\phi^2, \quad (4)$$

with the metric potentials $B = B(r)$ and $A = A(r)$ depending on the radial coordinate r only. Considering a charged isotropic fluid, the Maxwell-Einstein equations (in units such that $c = 1 = G$) furnish the following set of independent equations,

$$\frac{dq}{dr} = 4\pi\rho_e r^2\sqrt{A}, \quad (5)$$

$$\frac{dm}{dr} = 4\pi\rho r^2 + \frac{q}{r}\frac{dq}{dr}, \quad (6)$$

$$\frac{dp}{dr} = -(p+\rho)A\left(4\pi pr + \frac{m}{r^2} - \frac{q^2}{r^3}\right) + \rho_e\sqrt{A}\frac{q}{r^2}, \quad (7)$$

$$\frac{dB}{dr} = \frac{2B}{p+\rho}\left(\frac{q}{4\pi r^4}\frac{dq}{dr} - \frac{dp}{dr}\right), \quad (8)$$

where the potential metric A^{-1} assumes the form

$$A^{-1} = 1 - \frac{2m}{r} + \frac{q^2}{r^2}. \quad (9)$$

Functions $m = m(r)$ and $q = q(r)$ represent respectively the gravitational mass and the electric charge within a sphere of radius r, while $\rho_e = \rho_e(r)$ is the electric charge density, and $\rho = \rho(r)$ and $p = p(r)$ stand respectively for the energy density and the pressure of the fluid. Taking $q = 0$ in Eq. (7), the original TOV [5,6] equation is recovered.

To solve the set of equations (5)–(9), a set of boundary conditions needs to be furnished. At the center of the spheres, the chosen conditions are $q(r=0) = 0$, $m(r=0) = 0$, $p(r=0) = p_c$, $\rho(r=0) = \rho_c$, $\delta(r=0) = \delta_c$, and $\rho_e(r=0) = \rho_{ec}$. The surface of the object is found through the condition $p(r=R) = 0$. At this point, $r = R$, the interior solution joins smoothly to the exterior vacuum solution provided by the Reissner-Nordström metric, where $B(r) = A^{-1}(r) = 1\text{–}2M/r + Q^2/r^2$, with $M = m(R)$ and $Q = q(R)$.

B. The equation of state and charge density profile

In the present case there are four equations [Eqs. (5), (6), (7), and (9)] and six variables [$q(r)$, $A(r)$, $m(r)$, $\rho(r)$, $p(r)$, and $\rho_e(r)$], forming an incomplete set of equations. To close the system, as usual, an equation of state and, for the charged fluid, a relation defining the charge density profile need to be supplemented.

As stated earlier, the equation of state employed here is the relativistic polytropic equation (2). In the following, the equation of state (2) (EoS 2) and its respective results are called case 2, while (1) (EoS 1) and its respective results (already reported in Ref. [18]) are called case 1.

We also need an additional input regarding the electric charge distribution. For the sake of comparison with results of previous works, e.g., [15–18,36,37], we assume that the electric charge density is proportional to the energy density of the fluid,

$$\rho_e = \alpha\rho, \quad (10)$$

where α is a dimensionless constant that we call the charge fraction, which is constrained to the interval $\alpha \in [0, 1)$. Let us mention that other interesting choices could be made, e.g., a relation of the form $\rho_e = \alpha\delta$. Besides the strong reason of being the same relation as in the previous work [18], whose results we aim to compare with the present analysis, another reason to choose the form of Eq. (10) is that it has shown to produce more compact objects in comparison with other charge density profiles.

III. THE STRUCTURE OF RELATIVISTIC CHARGED POLYTROPIC SPHERES

A. General remarks

Here the structure of charged spheres is analyzed for different values of the exponent γ and for different values of δ_c. The only free parameter left is then the polytropic constant ω. Following Ref. [18], we take the polytropic constant as

$$\omega = \bar{\omega}\delta_0^{*1-\gamma}, \tag{11}$$

where the dimensionless polytropic constant is $\bar{\omega} = 1.47518 \times 10^{-3}$ and the normalization factor adopted during the numerical integration of the TOV equation is $\delta_0^* = 1.78266 \times 10^{15}$ [kg/m^3].

Once the values of α, γ, and δ_c have been fixed, the system of equations are solved numerically by using the fourth-order Runge-Kutta method.

For convenience of the numerical analysis we restore the gravitational constant, $G = 7.42611 \times 10^{-28}$ [m/kg], but keep the speed of light $c = 1$.

Along this section, we compare the equilibrium configurations of charged relativistic polytropes to the charged nonrelativistic polytropes studied in Ref. [18].

B. The radius against the mass for fixed polytropic exponent: The Chandrasekhar and the Oppenheimer-Volkoff limits

With the purpose of verifying the Chandrasekhar and the Oppenheimer-Volkoff limits for the relativistic EoS 2, Eq. (2), we check the behavior of the radii and the masses of the charged fluid spheres for the central rest-mass density in the interval 10^{13} [kg/m^3]$\leq\delta_c \leq 10^{20}$ [kg/m^3] and $\gamma = 4/3$ and $\gamma = 5/3$, in a similar way as done in [18]. We note that the curves built in case 2 are very similar to those ones found in case 1; cf. Figs. 1 and 2 of ALZ. Moreover, both the Chandrasekhar and the Oppenheimer-Volkoff limits appear for $\gamma = 4/3$ and only the Oppenheimer-Volkoff limit appears when $\gamma = 5/3$.

We find that, irrespective of the value of α used, when $\gamma = 4/3$ and $\gamma = 5/3$ the masses of nonrelativistic polytropes and relativistic polytropes are very close to each other for low and equal values of central energy densities (ρ_c) and central rest-mass densities (δ_c). The differences become more apparent when the value of $\rho_c = \delta_c$ is incremented. For example, in the case of $\gamma = 4/3$, $\alpha = 0.9$, and $\rho_c = \delta_c = 10^{20}$ [kg/m^3], the mass of the sphere in case 1 is 0.578740 $M_\odot$, and in case 2 it is 0.532140 $M_\odot$, a difference of about 8.052%. This result confirms that EoS 1 and EoS 2 are not equivalent for large values of energy (rest-mass) density, as expected. In turn, the charge to mass ratio Q/M does not vary by more than 2% being larger in EoS 1 case.

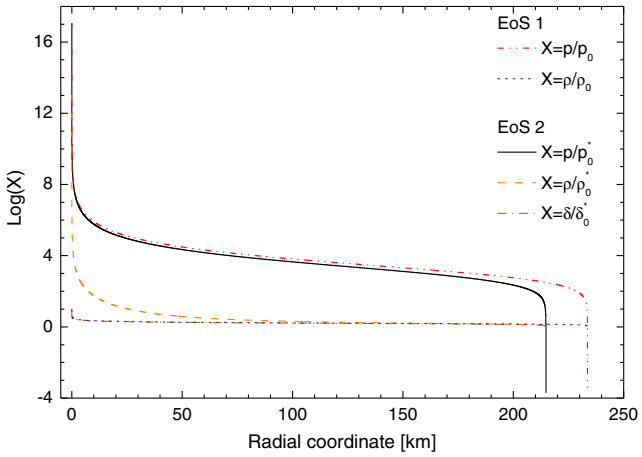

FIG. 1. The radial dependency of the normalized functions $p(r)/p_0$ and $\rho(r)/\rho_0$ with $\rho_c = 1.78266 \times 10^{16}$ [kg/m^3] for case 1, and $p(r)/p_0^*$, $\rho(r)/\rho_0^*$, and $\delta(r)/\delta_0^*$ with $\delta_c = 1.78266 \times 10^{16}$ [kg/m^3] for case 2. In both cases we have chosen $\alpha = 0.99$ and $\gamma = 17.0667$.

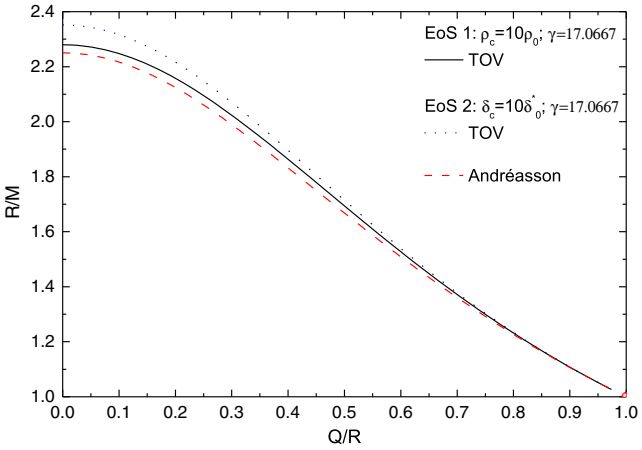

FIG. 2. The most compressed objects found numerically for EoS 1 with $\rho_c = 1.78266 \times 10^{16}$ [kg/m^3] and for EoS 2 with $\delta_c = 1.78266 \times 10^{16}$ [kg/m^3], as indicated. The Buchdahl-Andréasson bound is also shown for comparison (dashed line). This bound is saturated only in the limit of large charge fraction, $\alpha \to 1$, for which the quasiblack hole limit is reached.

C. The structure of relativistic charged spheres with varying polytropic exponent

1. General remarks

The dependence of the main physical properties of the charged fluid spheres as a function of the polytropic exponent γ is analyzed for a few values of α and for the fixed central rest-mass density $\delta_c = 1.78266 \times 10^{16}$ [kg/m^3], considering the relativistic polytropic equation of state (2). The polytropic exponent is taken in the interval

$4/3 \leq \gamma \leq 17.0667$. It is worth mentioning that the curves obtained in case 2 are similar to those derived in case 1 (cf. Sec. D of Ref. [18]); thereby, in the course of this subsection, we only mention the main differences between the two cases.

2. Radius of the relativistic spheres against the polytropic exponent

In the uncharged case, $\alpha = 0.0$, we find that the minimum value of the radius to mass ratio is approximately $R/M = 2.35182$. This value is found for large γ and it is just 3.2% larger than the one derived in case 1 (cf. Fig. 4 of ALZ). From this result we understand that by extrapolating the polytropic exponent γ to infinity, the upper limit of the Buchdahl bound is not attained, differently from case 1 where this limit is reached. The main point that may explain this different degree of compactness is that the central energy density is finite in case 1, while it diverges in case 2. Notwithstanding, in the extremely charged case, $\alpha = 0.99$, we have $R/M \simeq 1.02514$ for EoS 2, being only 0.16% lower than the ratio determined in case 1. This value of R/M is close to the maximum compactness of a charged object, $R/M = 1.0$. From this we understand that for large (infinite) values of γ the Buchdahl-Andréasson bound [23] is saturated in the limit $\alpha \to 1$.

3. Mass of the spheres against the polytropic exponent

For low values of γ, the masses found in case 2 are very close to the ones found in case 1. As found in [18], we note that the mass increases very fast with the polytropic exponent. The growth of the mass with the polytropic exponent γ is explained in the same way for both equations of state, since a larger central pressure p_c is obtained with a higher γ. For the fixed value of δ_c considered here, the masses of the relativistic polytropes (case 2) are of the order of 10% lower than the masses of the nonrelativistic stars (case 1, cf. Fig. 5 of ALZ).

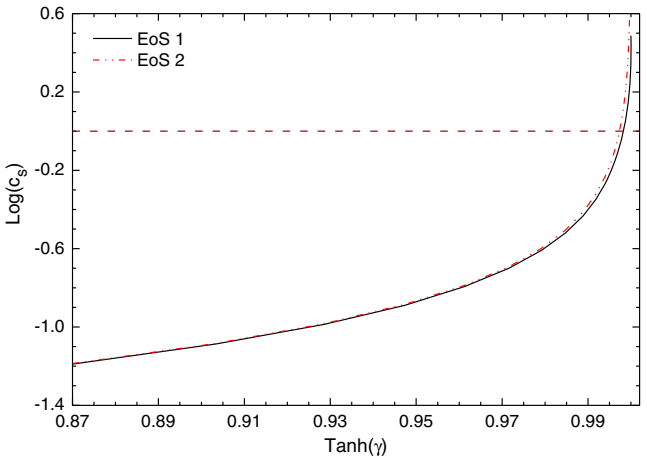

FIG. 3. The central speed of sound versus the polytropic exponent for EoS 1 and EoS 2.

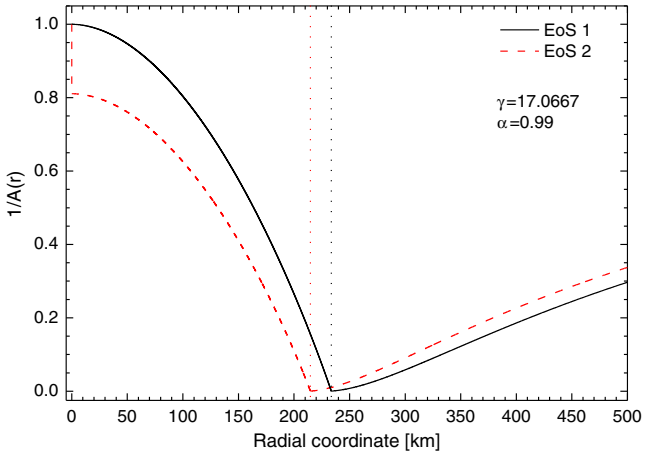

FIG. 4. The metric function $A^{-1}(r)$ against the radial coordinate for EoS 1 and EoS 2. The dotted vertical lines indicate the surface of the spheres.

4. Charge of the spheres against the polytropic exponent

The behavior of the charge to mass ratio (Q/M) as a function of the polytropic is also investigated. The results are very similar to EoS 1 case. In fact, for the typical central rest-mass density $\delta_c = 1.78266 \times 10^{16}$ [kg/m^3], the maximum difference in Q/M is of about 2.1×10^{-3}% higher for the relativistic polytropes (case 2) than the corresponding ratio for the nonrelativistic polytropes (case 1, cf. Fig. 6 of ALZ). Larger differences happen for larger values of δ_c. We note also that in the extreme case, with $\alpha = 0.99$ and $\gamma = 17.0667$, the values of the ratio Q/M are very close to unity indicating that the quasiblack hole regime is about to be reached. This point is investigated in detail in the next section.

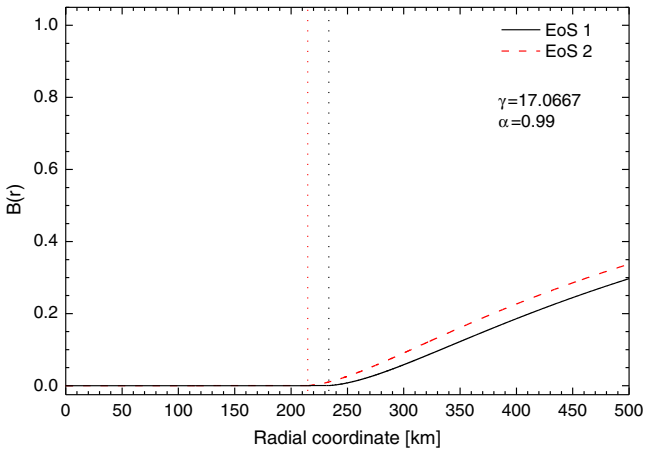

FIG. 5. The metric function $B(r)$ against the radial coordinate considering EoS 1 and EoS 2. The dotted vertical lines indicate the surface of the spheres.

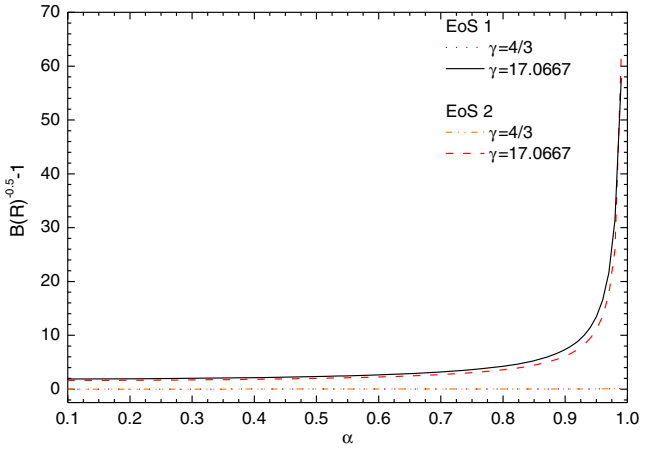

FIG. 6. The redshift function $B(R)^{-1/2}-1$ at the surface of the sphere as a function of the charge fraction for the nonrelativistic and relativistic polytropes.

D. The structure of relativistic charged spheres with varying charge fraction

We have also studied the dependence of the physical quantities of the relativistic charged polytropes with the charge fraction α. We analyzed the total mass, the radius, and charge as a function of α, and we found that the results are very similar to those built in EoS 1 case (cf. Sec. D of ALZ), with the main differences occurring for high energy densities. Due to this similarity, we do not show the respective graphics here.

IV. PROPERTIES OF RELATIVISTIC POLYTROPIC FLUID SPHERES WITH INFINITELY LARGE POLYTROPIC EXPONENT

A. Large polytropic exponent and incompressible fluids

In order to highlight the differences between the two equations of state, EoS 1 (1) and EoS 2 (2) for large values of γ, a comparison between them in the region of large fluid pressures must be performed.

The fluid quantities in the case of EoS 2 are normalized as p/p_0^*, ρ/ρ_0^* and δ/δ_0^*, where δ_0^*, ρ_0^* and p_0^* are normalization factors. These factors are related by $p_0^*=\omega\delta_0^{*\gamma}$ and $\rho_0^*=\delta_0^*+p_0^*/(\gamma-1)$. Hence, we get

$$\lim_{\gamma\to\infty}\frac{p}{p_0^*}=\lim_{\gamma\to\infty}\left(\frac{\delta}{\delta_0^*}\right)^{\gamma}=\begin{cases}0, & \text{if } \delta<\delta_0^*,\\ \infty, & \text{if } \delta>\delta_0^*,\end{cases} \tag{12}$$

and we have

$$\lim_{\gamma\to\infty}\frac{\rho}{\rho_0^*}=\lim_{\gamma\to\infty}\frac{\rho_e}{\rho_{e0}^*}=\begin{cases}\frac{\delta}{\delta_0^*}, & \text{if } \delta<\delta_0^*,\\ \infty, & \text{if } \delta>\delta_0^*,\end{cases} \tag{13}$$

where we used Eq. (11) with fixed $\bar{\omega}=1.47518\times10^{-3}$.

For the normalized rest-mass density we get

$$\lim_{\gamma\to\infty}\frac{\delta}{\delta_0^*}=\lim_{\gamma\to\infty}\left(\frac{p}{p_0^*}\right)^{1/\gamma}=1. \tag{14}$$

Therefore, differently from what happens in the case of EoS 1 [cf. Eqs. (18)–(20) of ALZ], the limit of high polytropic exponents of the relativistic equation of state (2) does not yield an incompressible fluid. It gives a constant rest-mass density, and in the instance when the pressure may assume arbitrarily large values, it gives an infinitely large energy density too, and in a second instance when the pressure vanishes it gives a constant energy density. This second situation results in charged dust matter, but it is not interesting for the present analysis.

Figure 1 shows the behavior of the normalized fluid quantities, the energy density $\rho(r)/\rho_0^*$, the pressure $p(r)/p_0^*$, and the rest-mass density $\delta(r)/\delta_0^*$ of the relativistic polytropic fluid (case 2) against the radial coordinate, with the central rest-mass density given by $\delta_c=10\delta_0^*=1.78266\times10^{16}\ [\mathrm{kg/m^3}]$. The normalization factors are $\delta_0^*=1.78266\times10^{15}\ [\mathrm{kg/m^3}]$, $p_0^*=2.62974\times10^{12}\ [\mathrm{kg/m^3}]$, and $\rho_0^*=1.78282\times10^{15}\ [\mathrm{kg/m^3}]$. For a clear comparison, we draw also the corresponding curves for case 1.

As seen from Fig. 1, the pressure presents the same behavior in both cases. On the other hand, the energy density for case 2 has a completely different behavior when compared to case 1. In case 1, the energy density is nearly constant, starting with $\rho(r)/\rho_0=10$ at $r=0$ and decreasing very slowly with r until the surface of the sphere at $r=R$, where it reaches its minimum value. For case 2, the energy density behaves like the pressure. It starts with the high value $\rho(r)/\rho_0^*=10^{13.0}$ at the center of the object and varies rapidly with the radial coordinate to reach a value close to zero at the surface of the object $r=R$. Finally, we see that the rest-mass density function is approximately a constant, starting with the value $\delta(r)/\delta_0^*=10$ at $r=0$ and decaying very slowly toward the surface of the sphere $r=R$.

B. Large polytropic exponents: The Buchdahl bound, the Buchdahl-Andréasson bound, and the quasiblack hole limit

The existence of upper bounds for compact objects is one of the remarkable predictions of general relativity. The upper limit established by Buchdahl [20] in the case of uncharged fluid spheres was extended to include electric charged fluid spheres by Andréasson [23]. Our main concern here is testing these bounds for the relativistic polytropic spheres. So, we search in the parameter space for the most compressed objects.

Figure 2 shows the behavior of the ratio R/M as a function of Q/M for the most compressed stellar static objects that follow from EoS 1 (solid line) with $\rho_c=1.78266\times10^{16}\ [\mathrm{kg/m^3}]$, and from EoS 2 (dotted

line) with $\delta_c = 1.78266 \times 10^{16}$ [kg/m^3]. The same central pressure $p_c = 2.62974 \times 10^{12}$ [kg/m^3] was used for both equations of state. The two curves are drawn for the highest value of the polytropic exponent that yielded trusted numerical results, $\gamma = 17.0667$. For the sake of comparison, the upper limit of the theoretical prediction by Andréasson (dashed line), which is given by relation (3), is also depicted in Fig. 2. Notice that the two curves for the polytropic spheres (the solid and the dotted curves) appear above the Buchdahl-Andréasson bound for all Q/R.

As seen from Fig. 2, in the limit of zero charge, $Q/R \to 0$, the ratio R/M approaches the upper limit of the Buchdahl bound $R/M \to 9/4 = 2.25$ better for the nonrelativistic polytropes (EoS 1) than for the relativistic polytropes (EoS 2). Noticing that the limit of infinitely high polytropic exponents yields an incompressible fluid in case 1, the previous results of Ref. [22] (see also [18]) assure us that the Buchdahl bound is saturated by the uncharged fluid spheres in such case, but not in the present case (case 2). The numerical calculation does not reach the ceiling value $R/M = 9/4$ since the method employed here does not allow us to go beyond $\gamma = 17.0667$. In fact, the values shown in Fig. 2 at $Q = 0$ are $R/M \simeq 2.35$ for EoS 2, and $R/M \simeq 2.28$ for EoS 1. Thus, the Buchdahl bound is not saturated by the uncharged fluid spheres with the relativistic polytropic equation of state (case 2).

On the other side of the parameter space, for large charge fractions, $\alpha \to 1$, the two curves for charged spheres converge to the Buchdahl-Andréasson line. This means that the two equations of state model very compressed objects that saturate the Buchdahl-Andréasson bound in such a limit. The three lines converge to the quasiblack hole limit $R = M = Q$. As a matter of fact, in the case analyzed here, the maximum value of the charge fraction is $\alpha = 0.99$ rather than $\alpha = 1.0$, since we have not found static equilibrium solutions (the numerical method does not converge) for α larger than 0.99. For this value of α we have found $R/M \simeq 1.02514$ in case 2 and $R/M \simeq 1.02676$ in case 1 (see Ref. [18]). Let us stress that in Fig. 2 the three lines showed are very close to each other in the region $Q/R \simeq 1.0$ but they do not coincide. The numerical results indicate that the three lines shall coincide just in the limit $\alpha \to 1$ with $\gamma \to \infty$.

V. THE SPEED OF SOUND IN RELATIVISTIC POLYTROPIC CHARGED SPHERES

The speed of sound in a compressible fluid is determined through the relation $c_s^2 = dp/d\rho$. For the relativistic polytropic equation of state (EoS 2), we get

$$c_s^2 = \frac{dp}{d\rho} = \frac{\gamma p}{\rho + p}. \tag{15}$$

Since the speed of sound decreases toward the surface of the sphere, as happens to the pressure, to see if the velocity of sound exceeds the speed of light it is only necessary to analyze the speed of sound in the center of the objects.

It is known that EoS 2 does not violate the constraint $c_s^2 \leq 1$ for large ρ. In fact, the limit of large energy densities yields $c_s^2 \to \gamma(\gamma - 1)/2$. One then sees that c_s^2 equals unity for $\gamma = 2$. Therefore, as also known, the relativistic equation of state does not violate causality for γ in the interval $1 \leq \gamma \leq 2$.

The dependence of the central (at $r \to 0$) speed of sound upon the polytropic exponent is shown in Fig. 3, where we plot the function (15) for the relativistic polytropic equation of state with $\delta_c = 1.78266 \times 10^{16}$[kg/m^3]. We determine that the speed of sound c_s in the center of the spheres reaches the speed of light at $\gamma \simeq 3.52364$ for EoS 2. It is 6.4% larger than the value found in case 1 (cf. Fig. 14 of ALZ).

Despite the fact that the sound speed surpasses the speed of light for sufficiently high values of the polytropic exponent γ, these solutions are interesting because, in such a limit, the fluids become incompressible and the quasiblack hole limit is reached.

VI. THE QUASIBLACK HOLE LIMIT OF A RELATIVISTIC POLYTROPIC CHARGED SPHERE

A. Basic properties and the quasiblack hole limit

It is verified that the relativistic polytropes (EoS 2) with central rest-mass density $\delta_c = 10\delta_0^* = 1.78266 \times 10^{16}$ [kg/m^3], charge fraction $\alpha = 0.99$, and polytropic exponent $\gamma = 17.0667$ are very close to the quasiblack hole configuration. Now we check if the limits $\alpha \to 1$ and $\gamma \to \infty$ really yield quasiblack holes. For this purpose, following the defining properties of a static quasiblack hole of Ref. [19], the potential metrics $A(r)$ and $B(r)$ are then analyzed.

The inverse of the metric function $A(r)$ versus the radial coordinate r is plotted in Fig. 4 for EoS 2, and, for comparison, the corresponding graph for EoS 1 is also drawn. It is seen that function $A^{-1}(r)$ decreases with the increasing of the radial coordinate, reaching its minimum value, namely, $A^{-1}(R) \sim 0$, at the surface of the object. Such a vanishing value signals that the object is close to a quasiblack hole configuration. The interior metric is matched to the exterior Reissner-Nordström metric, i.e., $A^{-1}(R) = 1 - 2M/R + Q^2/R^2$, from which it follows that the quasihorizon is present.

The metric function $B(r)$ versus radial coordinate is shown in Fig. 5 for EoS 2 and, for comparison, also for EoS 1. Function $B(r)$ assumes values close to zero in the interior of the sphere, i.e., $B(r) \to 0$ in the whole interval $0 \leq r \leq R$. This feature also reveals that we are close to the quasiblack hole configuration. Since the interior solution is matched to the exterior vacuum Reissner-Nordström solution, it follows

that we have $B(R) = A^{-1}(R) = 1–2M/R + Q^2/R^2 \sim 0$, confirming once again the presence of a quasihorizon.

Besides the defining properties of the metric potentials, as just checked, another important property of charged static quasiblack holes is the existence of extremal limits for the ratios Q/M and R/M. In the present case the numerical analysis shows that the extremal bound $Q/M = R/M = 1$ is continuously approached with the increasing of the polytropic exponent and, in particular, of the charge fraction α. Then, considering the two solutions of equation $F(r) = 1–2M/r + Q^2/r^2 = 0$, which are $r_\pm = M \pm \sqrt{M^2 - Q^2}$, we get $r_+ \simeq r_- \simeq M \simeq Q \simeq R$ (see Table I), confirming the presence of an extremal quasihorizon.

Lines B and C of Table I present the mass M, the charge Q, the radius R, and their relations for the relativistic polytropes (EoS 2) with $\alpha = 0.99$, and for two values of the polytropic exponent, $\gamma = 17.0667$ and $\gamma = 17.1109$, respectively. For values of γ higher than these, the numerical procedure presents convergence problems. For comparison, the same quantities for EoS 1 case are also listed in the table (row A). It is seen that R/M and Q/M are closer to unity in EoS 2 case than in EoS 1 case. Based on these results we note that the relativistic polytropic spheres with large polytropic exponents and charge fraction approaching unity attain the quasiblack hole limit faster than the nonrelativistic polytropic spheres.

B. The redshift at the surface of a quasiblack hole

For completeness, we calculate the quantity $B(R)^{-1/2} - 1$ for both the nonrelativistic and the relativistic charged polytropes as a function of the charge fraction, and taking two values of the polytropic exponent, $\gamma = 4/3$ and 17.0667, and central rest-mass density $\delta_c = 1.78266 \times 10^{16}$ [kg/m^3], the result being shown in Fig. 6. The charge fraction varies in the range $0 < \alpha < 1$. The expression $B(R)^{-1/2} - 1$ gives the redshift at the surface of the star, which is defined in the usual way by the fractional difference between the light wave frequency at the surface of the star (at $r = R$) with respect to infinity (at $r \to \infty$). As expected, the redshift at the surface of the polytropes in the quasiblack hole limit is infinitely large. Numerically we determine values of about 100 in the cases with $\alpha = 0.99$ and $\gamma = 17.0667$. Again the results for EoS 2 are very close to those for EoS 1 (see [22]), but the redshift is a little higher for the relativistic polytropes (EoS 2).

VII. CONCLUSIONS

The static stellar equilibrium configurations of uncharged and charged relativistic polytropic spheres were investigated in the Maxwell-Einstein theory. These results were compared with those of the nonrelativistic polytropic spheres analyzed in [18].

First the analysis was done by varying the central rest-mass density δ_c. A few different values of the polytropic exponent and of the charge fraction were considered in such an analysis. A detailed analysis of the equilibrium configurations was done by calculating the radius, the mass, and the charge of each configuration. The results found for EoS 2 (2) were very similar to those for EoS 1 (1); cf. Ref. [18]. The study also confirmed that the two equations of state yield significantly different results just in the limit of high energy densities.

The charge fraction parameter α was varied from zero to very close to unity, $\alpha = 0.99$. A value higher than this was also implied in numerical convergence problems. Again the structure of the resulting equilibrium solutions were almost the same for both models of fluids.

In the regime of high polytropic exponents γ, the main differences are related to the central energy density behavior, which goes with the pressure in EoS 2, while it is almost a constant in EoS 1 case. In such a limit, we also tested the various bounds for extremely compact objects. The surface redshifts of the extremely compact solutions, including the quasiblack hole limit, were analyzed. The results show higher redshifts for relativistic polytropes (EoS 2) than for nonrelativistic polytropes (EoS 1).

The dependence of the sound speed c_s on the polytropic exponent at the center of the compact objects was also studied. In both cases c_s reached values higher than the speed of light for sufficiently high polytropic indexes.

Finally, we emphasize once again that the aim of this work was to analyze the structure of relativistic polytropes by comparing to nonrelativistic polytropes, with particular interest in the upper bounds of compactness established within the theory of general relativity. This is a complement to previous works by us whose results were reported in Refs. [18,22]. The conclusion of this investigation is that the Buchdahl-Andréasson bound is not saturated in full either by polytropic stars or by incompressible stars. On the other hand, as shown in Ref. [24], that bound is saturated by

TABLE I. The values of the mass M, charge Q, and radius R of the charged polytropic spheres, in geometric units, with the corresponding values of R/M and Q/M, for $\alpha = 0.99$ and $\gamma = 17.0667$, are shown in rows A and B, respectively, for case 1 and case 2. The values of M, Q, R, R/M, and Q/M, for EoS 2 and $\gamma = 17.1109$ are shown in row C.

	EoS	γ	$M \times 10^5$ [m]	$Q \times 10^5$ [m]	$R \times 10^5$ [m]	R/M	Q/M
A	1	17.0667	2.27478	2.27431	2.33566	1.02676	0.999793
B	2	17.0667	2.09502	2.09463	2.14769	1.02514	0.999813
C	2	17.1109	2.09662	2.09623	2.14929	1.02512	0.999814

the Guilfoyle [25] solutions, which assume different conditions on the fluid quantities. This result suggests that a different equation of state for the charged fluid, associated to an alternative charge density profile, may lead to solutions that saturate that important bound, besides reaching the quasiblack hole limit. The analysis of such situations is left for future investigations.

ACKNOWLEDGMENTS

V. T. Z. thanks Fundação de Amparo à Pesquisa do Estado de São Paulo—FAPESP, Grant No. 2011/18729-1; Conselho Nacional de Desenvolvimento Científico e Tecnológico—CNPq, Brazil, Grant No. 308346/2015-7; and Coordenação de Aperfeiçoamento de Pessoal de Nível Superior—CAPES, Brazil, Grant No. 88881.064999/2014-01.

[1] A. S. Eddington, *The Internal Constitution of Stars* (Cambridge University Press, Cambridge, England, 1926).
[2] K. S. Thorne, Relativistic stellar structure and dynamics, in *High Energy Astrophysics (1966 Les Houches Summer School of Theoretical Physics)*, edited by C. DeWitt, E. Schatzmann, and P. Véron (Gordon and Breach, New York, 1967), Vol. III, p. 250.
[3] S. Chandrasekhar, The highly collapsed configurations of a stellar mass, Mon. Not. R. Astron. Soc. **91**, 456 (1931).
[4] S. Chandrasekhar, The highly collapsed configurations of a stellar mass (second paper), Mon. Not. R. Astron. Soc. **95**, 207 (1935); J. R. Oppenheimer and H. Snyder, On continued gravitational contraction, Phys. Rev. **56**, 455 (1939).
[5] R. C. Tolman, Static solution of Einstein's field equation for spheres of fluid, Phys. Rev. D **55**, 364 (1939).
[6] J. R. Oppenheimer and G. Volkoff, On massive neutron cores, Phys. Rev. D **55**, 374 (1939).
[7] R. F. Tooper, General relativistic polytropic fluid spheres, Astrophys. J. **140**, 434 (1964).
[8] R. F. Tooper, Adiabatic fluid spheres in general relativity, Astrophys. J. **142**, 1541 (1965).
[9] K. Mrázová, S. Hledík, and Z. Stuchlík, Games with polytropes and adiabates, in *Proceedings of RAGtime 6/7: Workshops on Black Holes and Neutron Stars*, edited by S. Hledík and Z. Stuchlík (Silesian University, Opava, 2005).
[10] S. C. Pandey, M. C. Durgapal, and A. K. Pande, Relativistic polytropic spheres in general relativity, Astrophys. Space Sci. **180**, 75 (1991).
[11] S. C. Pandey, M. C. Durgapal, and A. K. Pande, A study massive classical polytropes in general relativity, Astrophys. Space Sci. **159**, 203 (1989).
[12] S. Hledík, Z. Stuchlík, and K. Mrázová, Comparison of general relativistic polytropic and adiabatic spheres with repulsive cosmological constant, in *Proceedings of RAGtime 4/5: Workshops on Black Holes and Neutron Stars*, edited by S. Hledík and Z. Stuchlík (Silesian University, Opava, 2004).
[13] L. Herrera and W. Barreto, General relativistic polytropes for anisotropic matter: The general formalism and applications, Phys. Rev. D **88**, 084022 (2013).
[14] J. Bekenstein, Hydrostatic equilibrium and gravitational collapse of relativistic charged fluid balls, Phys. Rev. D **4**, 2185 (1971).
[15] J. L. Zhang, W. Y. Chau, and T. Y. Deng, The influence of a net charge on the critical mass of a neutron star, Astrophys. Space Sci. **88**, 81 (1982).
[16] S. Ray, A. L. Espíndola, M. Malheiro, J. P. S. Lemos, and V. T. Zanchin, Electrically charged compact stars and formation of charged black holes, Phys. Rev. D **68**, 084004 (2003).
[17] B. B. Siffert, J. R. De Mello, and M. O. Calvão, Compact charged stars, Braz. J. Phys. **37**, 609 (2007).
[18] J. D. V. Arbañil, J. P. S. Lemos, and V. T. Zanchin, Polytropic spheres with electric charge: Compact stars, the Oppenheimer-Volkoff and Buchdahl limits, and quasiblack holes, Phys. Rev. D **88**, 084023 (2013).
[19] J. P. S. Lemos and O. B. Zaslavskii, Quasiblack holes: Definition and general properties, Phys. Rev. D **76**, 084030 (2007).
[20] H. A. Buchdahl, General relativistic fluid spheres, Phys. Rev. **116**, 1027 (1959).
[21] K. Schwarzschild, Über das Gravitationsfeld eines Kugel aus inkompressibler Flüssigkeit nach der Einsteinschen Theorie, Sitzungsberichte der Königlich Preussischen Akademie der Wissenschaften **1**, 424 (1916).
[22] J. D. V. Arbañil, J. P. S. Lemos, and V. T. Zanchin, Incompressible relativistic spheres: Electrically charged stars, compactness bounds, and quasiblack hole configurations, Phys. Rev. D **89**, 104054 (2014).
[23] H. Andréasson, Sharp bounds on the critical stability radius for relativistic charged spheres, Commun. Math. Phys. **288**, 715 (2009).
[24] J. P. S. Lemos and V. T. Zanchin, Sharp bounds on the radius of relativistic charged spheres: Guilfoyle's stars saturate the Buchdahl-Andréasson bound, Classical Quantum Gravity **32**, 135009 (2015).
[25] B. S. Guilfoyle, Interior Weyl-type solutions of the Einstein-Maxwell field equations, Gen. Relativ. Gravit. **31**, 1645 (1999).
[26] F. De Felice, L. Siming, and Y. Yunqiang, Relativistic charged spheres: II. Regularity and stability, Classical Quantum Gravity **16**, 2669 (1999).
[27] F. De Felice, Y. Yu, and J. Fang, Relativistic charged spheres, Mon. Not. R. Astron. Soc. **277**, L17 (1995).
[28] P. Anninos and T. Rothman, Instability of extremal relativistic charged spheres, Phys. Rev. D **65**, 024003 (2001).
[29] J. P. S. Lemos and E. J. Weinberg, Quasiblack holes from extremal charged dust, Phys. Rev. D **69**, 104004 (2004).
[30] W. B. Bonnor and S. B. P. Wickramasuriya, Are very large gravitational redshifts possible?, Mon. Not. R. Astron. Soc. **170**, 643 (1975).

[31] F. I. Cooperstock and V. de la Cruz, Sources for the Reissner-Nordström metric, Gen. Relativ. Gravit. **9**, 835 (1978).
[32] P. S. Florides, The complete field of charged perfect fluid spheres and of other static spherically symmetric charged distributions, J. Phys. A **16**, 1419 (1983).
[33] J. P. S. Lemos and V. T. Zanchin, Quasiblack holes with pressure: Relativistic charged spheres as the frozen stars, Phys. Rev. D **81**, 124016 (2010).
[34] J. P. S. Lemos and V. T. Zanchin, Plethora of relativistic charged spheres: The full spectrum of Guifoyle's static, electrically charged spherical solutions, Phys. Rev. D **95**, 104040 (2017).
[35] J. P. S. Lemos and O. B. Zaslavskii, Quasiblack holes with pressure: General exact results, Phys. Rev. D **82**, 024029 (2010).
[36] J. D. V. Arbañil and M. Malheiro, Equilibrium and stability of charged strange quark stars, Phys. Rev. D **92**, 084009 (2015).
[37] J. P. S. Lemos, F. J. Lopes, G. Quinta, and V. T. Zanchin, Compact stars with a small electric charge: The limiting radius to mass relation and the maximum mass for incompressible matter, Eur. Phys. J. C **12**, 3456 (2015).